Chapter 3

Structure of the Asymmetric Ripple Phase

3.1 Introduction

In this chapter we present electron density maps of various lipids (namely, DMPC, POPC, DHPC and DLPC) in the $P_{\beta'}$ phase. In section-3.2 we discuss our motivation for the present study. In section-3.3 we discuss the structure of the ripple phase inferred from the electron density maps of DMPC. We argue that all the features of the electron density maps are compatible with a tilt of the chains along the rippling direction. In section-3.4, we discuss the ripple shape and the temperature dependence of ripple parameters in POPC, DHPC and DLPC. In section-3.5 we discuss the influence of chirality on the ripple profile and show that molecular chirality does not affect the shape of the ripples. Our results are summarized in section-3.6.

3.2 Motivation

Though some of the structural aspects of the ripple phase were well established [1, 2, 3, 4, 5, 6] the finer features were poorly understood when we started our studies on this phase. The ordering of the hydrocarbon chains within the bilayer is one such feature. Though as mentioned in chapter-I, the chains are mostly stiff and have some sort of positional order [2], diffusion and NMR experiments indicate that there is considerable amount of disorder associated with the chain region [7, 8]. The nature of this disorder is still a matter of debate. Empirically, only lipids that have a $L_{\beta'}$ phase

at lower temperatures exhibit the ripple phase [1], indicating the importance of the tilt of the chains in the formation of the ripples [10].

Though it is clear from x-ray data that the chains are tilted in the $P_{\beta'}$ phase [2], the direction of this tilt is not known. The chain reflections recorded in experiments are rather broad and therefore it has not been possible to obtain the tilt of the chains in the ripple phase directly from x-ray data. This broadening of the chain reflections happens because of one or both of the following reasons: the presence of disordered chains can broaden the spots or there might be an inherent spread in the spots because of the fact that the chains are arranged on a rippled bilayer rather than on a flat bilayer.

Many of the theories of the ripple phase are based on models where the tilt of the chains play an important role. For example, the Chen-Lubensky-MacKintosh model [11, 12] (see chapter-V) forbids a tilt of the chains along the rippling direction, and the Seifert-Shillock-Nelson model [13] (see chapter-V) is based on the idea that the tilt in the two monolayers of the bilayer are decoupled. Therefore determining the direction of the chain tilt should provide some important clues to construct a theory of the ripple phase.

Recently, Sun et. al. [14], have calculated the electron density. map of DMPC in the ripple phase from the x-ray data of Wack and Webb [15]. This map shows a saw-tooth shaped ripple profile. They find that: (a) the bilayer thickness in the smaller arm of the saw-tooth is smaller than that in the longer arm and is comparable to the bilayer thickness in the L_α phase. The bilayer thickness in the longer arm is found to be about the same as that in the $L_{\beta'}$ phase. (b) The electron density in the head-group region is similarly lower in the smaller arm. Based on the above observations they hypothesized that the chains in the longer arm of the ripple are

[1]DHPC is an exception. At high hydrations and low temperatures, it has an interdigitated gel phase (L_{β_I}) rather than a tilted gel phase ($L_{\beta'}$) but at higher temperatures it has a $P_{\beta'}$ phase [9]

stretched like in the $L_{\beta'}$ phase, whereas the shorter arm has disordered L_α like chains.

However, the above scenario is incompatible with other experimental observations. One such example is the diffusion experiment of Schneider et. al. [8]. In these experiments, self-diffusion in the ripple phase is found to be highly anisotropic, with a fast component that is 4-5 orders of magnitude faster than the slow component; but the fast component itself is about 2-3 orders of magnitude smaller than that in the L_α phase. Thus the authors of Ref. [8] conclude that although the intramolecular hydrocarbon chain disorder may be substantial in the fast bands, the intermolecular order in this region is not like that in the L_α phase.

Another compelling evidence against the L_α - $L_{\beta'}$ micro-phase-separation picture is from calorimetric data (this argument was first discussed by Carlson and Sethna [16]). The ratio of the lengths of the two arms of the ripple, as observed in the electron density map is about 1:2. Therefore according to the micro-phase-separation picture, at the L_α to $P_{\beta'}$ phase transition (the main-transition), about $\frac{2}{3}$ of the chains become all-*trans*. The rest of the chains can go to the all-*trans* conformation either gradually thus giving rise to a temperature dependence of the ratio of the lengths of the two arms or abruptly at the $P_{\beta'}$ to $L_{\beta'}$ transition (the pre-transition). Our experiments (discussed later in this chapter) rule out a temperature dependence of the ratio of the two arms. Therefore $\frac{1}{3}$ of the chains should go from L_α like to $L_{\beta'}$ like configuration at the pre-transition. This should imply that the ratio of the latent heat of the main-transition to the latent heat of the pre-transition should be roughly 2:1. But the ratio observed is about 10:1. Thus the micro-phase-separation picture is incompatible with diffusion and calorimetric experiments.

One of the motivations for recalculating the electron density maps of DMPC was to see if the results of Sun et. al. [14] was an artifact of their initial model for the trans-bilayer electron density profile. In their model, by construction, the bi-

layer thickness is different in the two arms of the ripple. It is partly to account for this features that they propose the micro-phase-separation model. Therefore it was important to check the correctness of the electron density maps they obtained, before attempting to explain the maps in terms of an alternative structure of this phase.

Though for a long time it was clear from x-ray and freeze fracture data that the stable ripples seen in experiments are asymmetric (without a mirror plane normal to the rippling direction), the actual shape of the ripples was not well established. A recent freeze fracture experiment [17] showed that the ripples have a profile that can be described by

$$h(x) = a\ cos(qx) + b\ cos(2qx) \tag{3.1}$$

where $h(x)$ describes the ripple profile along the rippling direction $\hat{x}$, q is the wave-number and a and b are constants. The ripple shape was thus predicted to be rather smooth. On the other hand, the electron density map of Sun. et. al. exhibit a less smooth, saw-tooth like profile. But since this initial model for fitting the ripple profile was also a saw-tooth, checking the model independence of the shape of the ripple was another objective of our analysis.

In previous work, the deviation of the unit cell parameter γ from $\frac{\pi}{2}$ (see chapter-II for the definition of γ) was always taken to be a direct indication of the asymmetry of the ripple profile. We argue that this need not necessarily be correct. The word asymmetric (symmetric) is used to indicate the absence (presence) of a plane of reflection in a direction perpendicular to the ripple wave-vector. A distinction should be made between the symmetry of the ripple profile (by which we mean the height variation of the bilayer) and the symmetry of the rippled bilayer itself. For concreteness consider a saw-tooth/triangular profile: the arguments presented here hold for a more smooth (sinusoidal like) profile also. In previous work, $\gamma = \frac{\pi}{2}$ was assumed to imply ripples where the lengths of the two arms are equal (symmetric profile) and $\gamma \neq \frac{\pi}{2}$ was assumed to imply ripples where the two arms are of unequal length (asymmetric

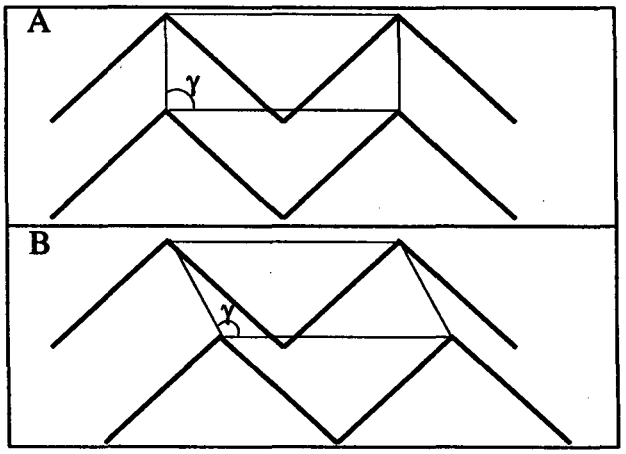

Figure 3.1: **A: The ripple profile is triangular with two equal arms and $\gamma = \frac{\pi}{2}$. B: The two arms of the ripple are still equal but now $\gamma \neq \frac{\pi}{2}$**

profile). But this assumption is valid only when the layer thickness in the two arms is the same (see figure-3.1). If the layer thickness is allowed to be different in the two arms, a symmetric profile (with two arms equal) is possible even when $\gamma \neq \frac{\pi}{2}$. Therefore, to ascertain the symmetry of the ripple profile, it is not enough to look at γ; it is necessary to get the actual shape of the profile.

In the absence of complete structural information, a theory of the ripple phase that explains all the experimental observations is difficult to formulate. Lubensky and MacKintosh [11, 12] proposed a Landau theory that predicts the formation of an asymmetric ripple phase in chiral bilayers. In this theory, the tilt of the hydrocarbon chains is the order parameter and a coupling between the divergence of the tilt and the mean membrane curvature can give rise to a height modulation of the bilayer. In the case of achiral bilayers, this model predicts the existence of two symmetric ripple phases in addition to a square lattice phase. When the system is chiral, one of these two phases becomes asymmetric. Thus, according to this phenomenological model, achiral bilayers can exhibit only symmetric ripples, whereas both symmetric and asymmetric ripples can occur in chiral bilayers [11, 12] (see chapter-V for detailed discussions). In order to test these predictions concerning the influence of molecular chirality on the structure of the ripple phase, Katsaras and Raghunathan

[19] carried out x-ray diffraction experiments on aligned films of chiral (*l*) and racemic (*dl*) dimyristoylphosphatidylcholine (DMPC) bilayers.

The experiments were done on a racemic mixture rather than a pure achiral compound because of the following reason. An organic molecule is chiral if it has atleast one carbon atom which is attached to four different groups. From figure-1.1 (chapter-I) it is clear that the carbon atom in 2 position in the backbone of a DMPC molecule has four different groups attached to it and hence DMPC is chiral. The achiral version of this molecule is 1,3 DMPC where the chains are attached to carbons 1 and 3 and the head-group is attached to carbon 2. This compound does not have a ripple phase (and incidentally has a L_{β_I} phase rather than a $L_{\beta'}$ phase at lower temperatures). Therefore in order to investigate the influence of chirality, it is necessary to look at racemic mixtures.

Under similar experimental conditions, the diffraction patterns from the chiral and racemic DMPC in the $P_{\beta'}$ phase were practically indistinguishable. Moreover, both the systems were found to have an oblique unit cell, which was taken as an indication of the presence of asymmetric ripples.

The observation of asymmetric ripples in the racemate can still be reconciled with the predictions of the Lubensky-MacKintosh model if the *d* and *l* enantiomers within each layer phase separate into chiral domains. To investigate this possibility, Katsaras et. al. performed calorimetric measurements on mixtures of *l*-dipalmitoylphosphatidylcholine having perdeuterated hydrocarbon chains (*l*-DPPC-d_{62}) and *d*-DPPC [20]. The main-transition in these mixtures is analogous to liquid to solid transitions. The calorimetric behavior of such mixtures can be any one of the following:

- A mechanical mixture or conglomerate: such mixtures exhibit one eutectic point. The mixture in the solid phase ($P_{\beta'}$ in this case) consists of crystallites of the two enantiomers.

- Racemic compound: molecules of the *d* and the *l* enantiomers get closely associated to form a compound. Such mixtures exhibit two eutectic points.

- Solid solution: the mixture is homogeneous and the two enantiomers are present unordered in the solid phase. The phase diagram has no eutectic point. The melting point gradually changes as the concentration is varied.

The data for *l*-DPPC-d_{62} and *d*-DPPC is consistent with a binary system whose components exhibit complete mutual solid solubility. This suggests that the asymmetric ripples seen in racemic DMPC multibilayers are not the result of the formation of chiral domains due to separation of the two enantiomers.

As mentioned in chapter-II, the wavelength of the ripples (λ_r), the bilayer periodicity (d) and the angle (γ) between the two axes of the unit cell are structural features that can be obtained directly from a diffraction pattern of oriented samples. The values of these three parameters are found to be comparable in chiral and racemic DMPC bilayers under similar experimental conditions. But as explained before, it is necessary to look at the detailed structure of the ripples to ascertain the shape of the ripple profiles. In order to check whether the detailed shape of the ripples in these two systems are also similar, we have calculated the electron density profiles of the ripple phase of *l* and *dl*-DMPC.

3.3 Electron density map of DMPC

3.3.1 The model

The data from Ref. [15] was fitted using three different models for $T_\psi(x,z)$ (see chapter-II). For powder samples of DMPC [15], models I, II and III give the same phases except for the faint (0,k) reflections [2]. Model III gives only a marginally better fit than model II. The values of L (L is the layer thickness along a direction making

[2] the phases are different for the faint reflection (3,0) also.

an angle ψ with the z-axis : see chapter-II for details) in the two arms are almost the same and comparable to that obtained from model II. This is also true of the other parameters which are allowed to be different in the two arms. However, model III gives a slightly higher value of 0.7 for f_1 (f_1 is the ratio of the electron density in the shorter arm to that in the longer arm). As discussed below, this factor can be accounted for in terms of the chain tilt, without resorting to the assumption of a L_α-like organization in the minor arm. The low Σ ($=\sum_{h,k} \mid\mid F_e^{hk} \mid - \mid F_o^{hk} \mid\mid^2$) and R ($=\frac{\sum_{h,k} \mid\mid F_e^{hk}\mid - \mid F_o^{hk}\mid\mid}{\sum_{h,k}\mid F_o^{hk}\mid}$) values for models II and III, and the absence of any physically unacceptable features in the electron density map (figure-3.2) indicate that these models closely represent the true structure of the system. The observed structure factors and those calculated using the three different models are given in table-3.1 and the converged values for the model parameters are given in table-3.2.

3.3.2 Existence of average tilt of the chains along the ripple

The electron density map of the ripple phase of DMPC, calculated with the data of [15] is shown in figure-3.2. The ripples clearly have a saw-tooth shape, with an offset between the two leaves of the bilayer. The simplest explanation for this offset is an average tilt of the chains along the rippling direction; such an offset cannot be expected if the tilt were in a plane normal to the rippling direction. The tilt angle ψ is found to be approximately equal to (γ-$\frac{\pi}{2}$). Further confirmation of the existence of an average tilt along this direction comes from the fact that the value of L (the layer thickness along ψ) is almost equal in the two arms and is comparable to twice the length of a fully stretched DMPC molecule (37.6 Å [21]). If it is assumed that the chains are tilted at an angle ψ with the z-axis, their tilt with respect to the local layer normal can be calculated from the shape of the ripple. Using the values of the structural parameters given in table-3.2, the tilt angle with respect to the local layer normal turns out to be 1.6^o and 34.5^o in the longer and shorter arms, respectively. The tilt in the short arm is comparable to that found in the $L_{\beta'}$ phase. Since the

Table 3.1: **Observed [| $F_o(h,k)$ |] and calculated [$F_c(h,k)$] structure factors obtained using the three models:** DMPC powder data at 18.2°C and partial specific volume of water = 0.263. Data from [15].

h	k	$\mid F_o(h,k) \mid$	$F_c(h,k)$		
			Model I	Model II	Model III
0	1	5.3	-1.7	9.2	8.5
0	2	9.7	1.2	-5.8	-3.1
0	3	7.8	-0.7	1.9	-2.2
1	-1	60.8	-99.3	-60.2	-59.3
1	0	100.0	-49.0	-99.7	-100.9
1	1	26.9	41.6	26.5	26.2
1	3	7.6	17.4	2.9	5.4
2	-2	15.1	-71.6	-12.5	-16.2
2	-1	71.2	-34.1	-71.4	-70.1
2	0	39.7	-11.6	-43.3	-44.1
2	1	33.9	29.2	31.7	31.3
2	2	22.7	-24.8	-22.7	-21.5
2	3	14.2	19.2	14.2	14.1
2	4	7.8	-13.2	-7.3	-9.6
3	-2	29.3	43.6	27.6	29.0
3	-1	44.2	28.1	45.7	44.3
3	0	12.0	-3.0	2.9	3.8
3	2	10.5	12.7	14.4	14.2
3	3	14.9	-14.8	-13.1	-12.5
3	4	10.0	14.0	9.6	9.8

Table 3.2: **The values of the structural parameters obtained from the three models.** DMPC powder data at 18.2°C and partial specific volume of water = 0.263. 2D-oblique lattice parameters are: λ_r=141.7 Å, d=58.6 Åand γ=98.4°. (Data from [15].)

Parameter	Model I	Model II	Model III
A_r(Å)	19.7	18.7	19.1
λ_1(Å)	106.2	101.0	101.5
ψ	5.7°	9.9°	9.1°
L(Å)	41.0	37.0	37.2,37.0*
ρ_h/ρ_m	1.1	0.9	1.1,1.1*
f_1	-	0.6	0.7
f_2	-	0.9	0.65
σ_h	-	4.9	4.6,4.7*
σ_m	-	13.3	9.4,10.0*
w(Å)	-	2.0(fixed)	9.2
Σ	692.5	217.6	213.6
R	0.172	0.083	0.087

* indicates the values in the shorter arm

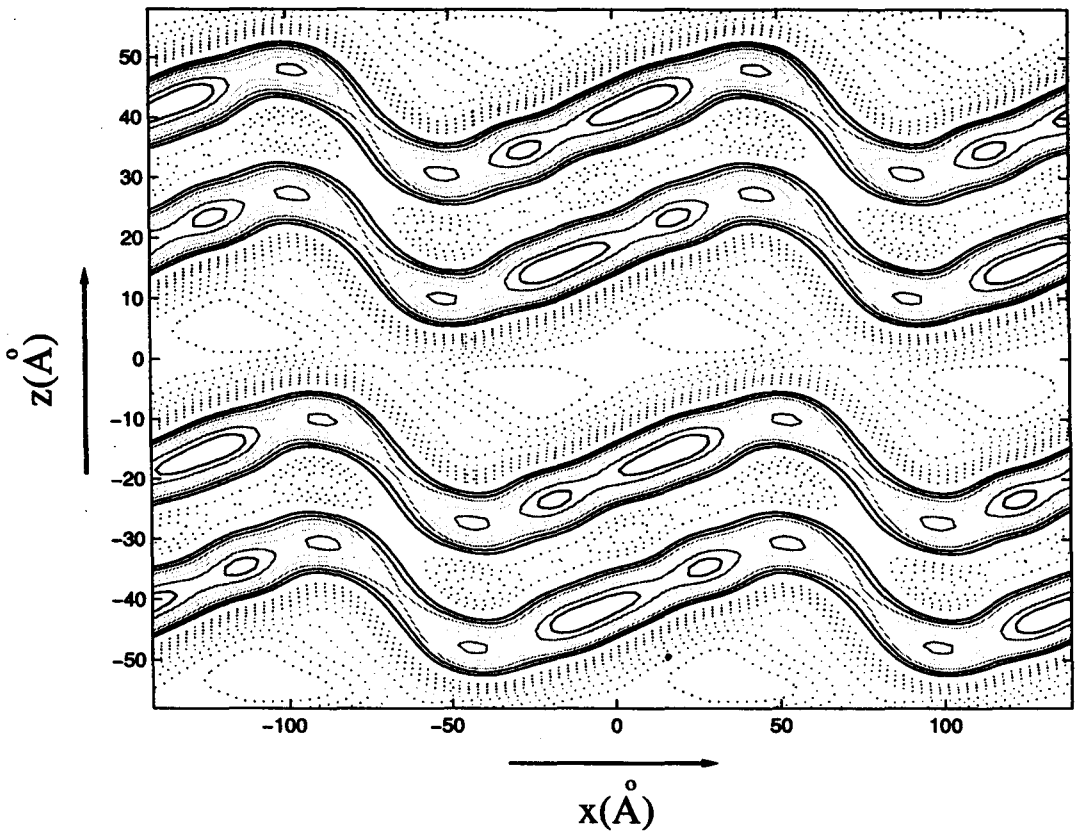

Figure 3.2: **Electron Density Map of the ripple phase of DMPC.** Temperature = 18.2°C and partial specific volume of water = 0.263 (Data from [15]). The positive (negative) contours are represented by solid (dotted) lines. The regions with positive electron density correspond to the head-groups. Note that the thickness of the bilayers is about 40 Å, whereas that of the water region is about 15 Å.

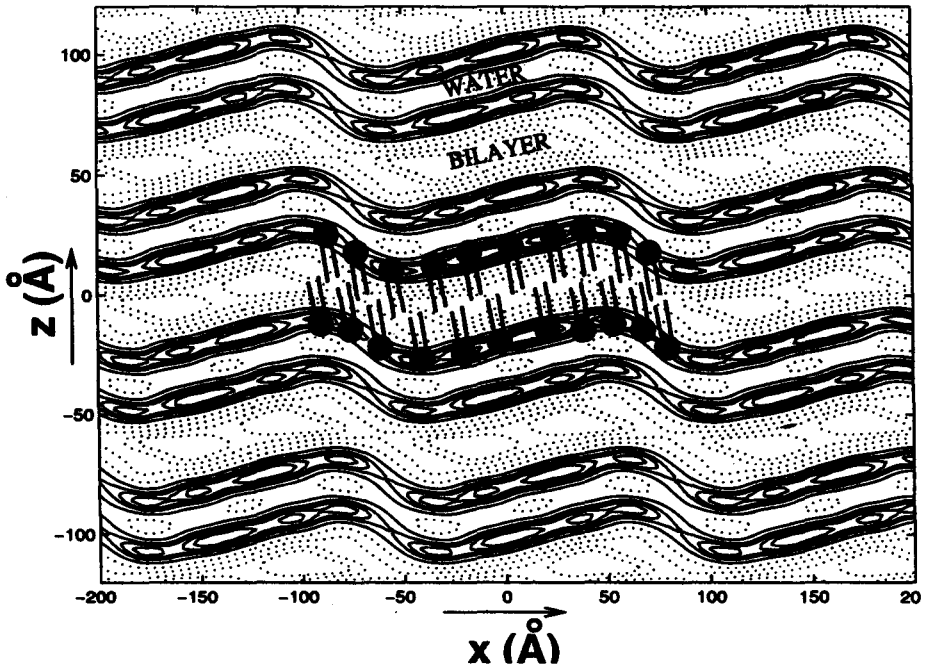

Figure 3.3: **The arrangement of the lipid molecules in the ripple phase.** The electron density map is same is in figure 3.2

area per molecule is inversely proportional to the cosine of this angle, a value of 0.82 is obtained for f_1. This is in very good agreement with the value of 0.77 obtained from the map for the ratio of the average electron densities in the head-group region of the longer and shorter arms. Thus an average tilt of the chains along the rippling direction provides a consistent explanation for many features of the electron density map. This means that to a good approximation the height modulation of the bilayers along the x-axis can be described as arising from a relative sliding movement of neighboring chains, with all the chains lying the x-z plane and tilted by a constant angle ψ with respect to the z-axis (see figure-3.3). The existence of an average chain tilt along the rippling direction breaks the reflection symmetry of the bilayer in the plane normal to it and hence can be expected to be responsible for the asymmetric ripples seen in this system.

We have confirmed that even if the initial model for the ripple profile is taken to be a more smooth sinusoidal-like shape (eq.-2.9), the final electron density map is still saw-tooth like. We find that the phases are insensitive to the precise details of

Table 3.3: **The structural parameters for DMPC at different temperatures.**

T (°C)	λ_r (Å)	d (Å)	γ (°)	λ_1 (Å)	A_r(Å)
25	140±2	55.6±0.1	99±1	90±1	19±1
24	142	55.8	99	91	20
23	142	55.9	100	88	19
22	144	56.0	100	87	19
21	145	56.3	99	95	20
20	154	56.4	99	98	20

initial shape chosen for $u(x)$. This indicates that the saw-tooth shape obtained for the ripple profile is not an artifact of the initial model. But if the initial shape is very different from the actual shape, for example if $u(x)$ is chosen to be a simple sinusoidal function, then the fit is very bad and the final electron density map has a lot of obviously unphysical features like discontinuity of bilayers.

3.3.3 Temperature dependence

We have also calculated the electron density maps of DMPC at different temperatures in the ripple phase, using data from oriented films. The structural features of the ripples are found to be similar to those obtained from the data of Ref.- [15]. The temperature dependence of the structural parameters of the ripples in DMPC are found to be very weak (table-3.3), as in the case of DPPC [18]. Contrary to results of freeze fracture experiments [17], we find that in all the cases studied, the ripple shape has Fourier components higher than the second. Further, we do not find a significant temperature dependence of the amplitude of the ripples, again in contrast to the results of ref.- [17]. The electron density map of DMPC at different temperatures is given in figures-3.4 and 3.5. The observed and calculated structure factors corresponding to the figures is given in table-3.4 and the converged values of the fitted parameters are given in table-3.5. The values of Σ and R for these fits are about 3500 and 0.3 respectively.

Table 3.4: **The observed and calculated structure factors for oriented sample of DMPC at different temperatures.**

		25°C		24°C		23°C		22°C		21°C		20°C	
h	k	$\|F_o\|$	F_c	$\|F_o\|$	F_c	$\|F_o\|$	F_c	$\|F_o\|$	F_c	$\|F_o\|$	F_c	$\|F_o\|$	F_c
1	0	100.0	-85.4	100.0	-80.2	100.0	-77.8	100.0	-78.0	100.0	-79.3	100.0	-84.8
1	-1	44.8	-39.8	42.5	-38.0	43.0	-37.3	-	-	48.6	-40.4	49.4	-40.7
1	1	-	-	-	-	-	-	42.2	38.0	-	-	-	-
2	0	31.3	-20.9	29.7	-19.8	28.8	-23.1	26.9	-21.5	28.9	-20.1	28.1	-21.6
2	-1	50.2	-42.1	43.6	-40.5	42.5	-38.2	41.6	-38.8	49.2	-43.4	49.4	-47.8
2	-2	10.2	-15.9	9.3	-15.4	9.5	-14.1	9.1	-16.6	12.5	-16.1	15.1	-20.7
2	2	17.5	-14.6	15.7	-14.6	15.9	-22.2	14.9	-15.6	17.1	-19.3	16.4	-16.6
2	3	13.7	7.7	10.6	7.9	10.9	13.3	8.3	7.5	11.1	12.6	13.0	8.4
3	0	24.1	-2.6	21.2	-2.9	21.0	-1.8	20.4	-1.7	23.6	-5.6	25.3	-4.8
3	-1	46.4	34.9	42.4	33.9	40.2	31.7	37.5	33.6	42.2	38.6	42.5	36.8
3	-2	30.6	32.5	29.2	32.0	28.4	28.9	27.6	32.4	31.7	37.8	33.6	38.2
3	2	10.0	17.1	9.5	17.1	-	-	22.3	21.2	30.2	20.9	-	-
3	3	18.0	-15.4	16.5	-15.9	27.6	-21.0	13.5	-17.9	15.2	-22.4	12.3	-18.3
3	4	17.2	9.7	16.3	10.3	17.8	13.3	14.1	9.7	15.7	17.4	15.9	11.4
3	5	-	-	12.4	-4.3	10.7	-4.4	12.3	-2.3	13.8	-9.4	12.9	-4.2
3	6	-	-	-	-	-	-	-	-	14.5	2.3	-	-
4	0	32.1	29.5	29.9	27.9	29.0	25.9	28.0	26.3	32.0	27.7	33.6	29.5
4	-1	30.1	-34.5	25.5	-31.2	23.3	-30.2	21.6	-29.0	22.7	-26.5	25.5	-26.0
4	-2	59.1	-84.3	55.5	-79.5	56.2	-75.6	52.5	-71.5	59.9	-81.4	60.1	-79.9
4	-3	29.4	-35.1	27.7	-33.9	26.9	-36.9	27.1	-35.9	31.4	-37.2	33.2	-40.4
5	0	10.6	0.3	8.5	0.6	7.7	3.0	6.8	1.6	6.9	1.7	5.9	1.7
5	-1	6.9	0.6	5.9	0.9	7.3	1.3	-	-	4.9	2.2	6.1	2.8
5	-2	-	-	7.8	-10.1	8.7	-10.6	8.5	-11.7	8.8	-12.8	8.7	-16.6
5	-3	-	-	-	-	8.7	-12.0	10.2	-17.6	10.2	-17.8	-	-
6	0	4.9	0.9	4.4	1.2	4.2	1.1	3.3	0.9	3.7	3.4	3.4	2.6
6	-1	5.9	-4.9	5.9	-5.4	4.7	-6.4	-	-	-	-	5.3	-7.9
6	-2	-	-	-	-	-	-	8.2	7.1	-	-	-	-
6	-3	-	-	-	-	9.9	21.8	-	-	-	-	-	-
7	0	-	-	-	-	2.4	-16.9	-	-	3.5	-17.5	-	-
9	0	-	-	-	-	2.1	-0.1	-	-	-	-	3.1	0.3

Table 3.5: **Converged values of the fitted parameters for DMPC at different temperatures.**

	25°C	24°C	23°C	22°C	21°C	20°C
λ_1(Å)	89.8	91.3	87.8	87.5	94.9	97.6
A_r(Å)	19.4	19.6	19.2	19.2	20.5	20.3
ψ	5.7°	5.7°	11.4°	5.7°	5.7°	2.8°
ρ_H/ρ_M	1.4	1.5	1.4	1.5	1.6	1.5
L(Å)	40.2	40.2	40.2	40.2	40.2	40.2

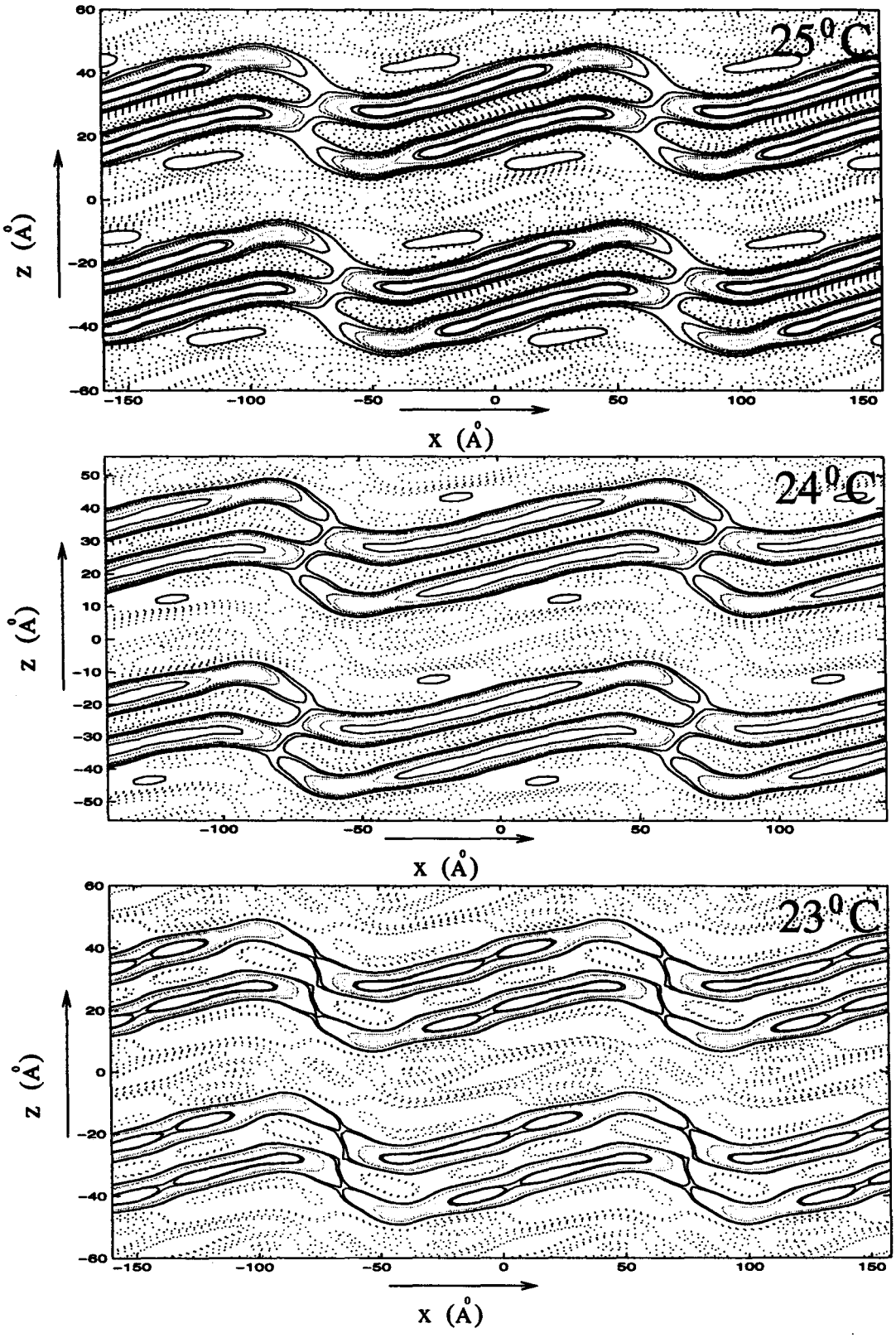

Figure 3.4: **Electron Density Map of the ripple phase of l-DMPC at different temperatures** The positive (negative) contours are represented by solid (dotted) lines. The regions with positive electron density correspond to the head-groups. Note that the thickness of the bilayers is about 40 Å, whereas that of the water region is about 15 Å.

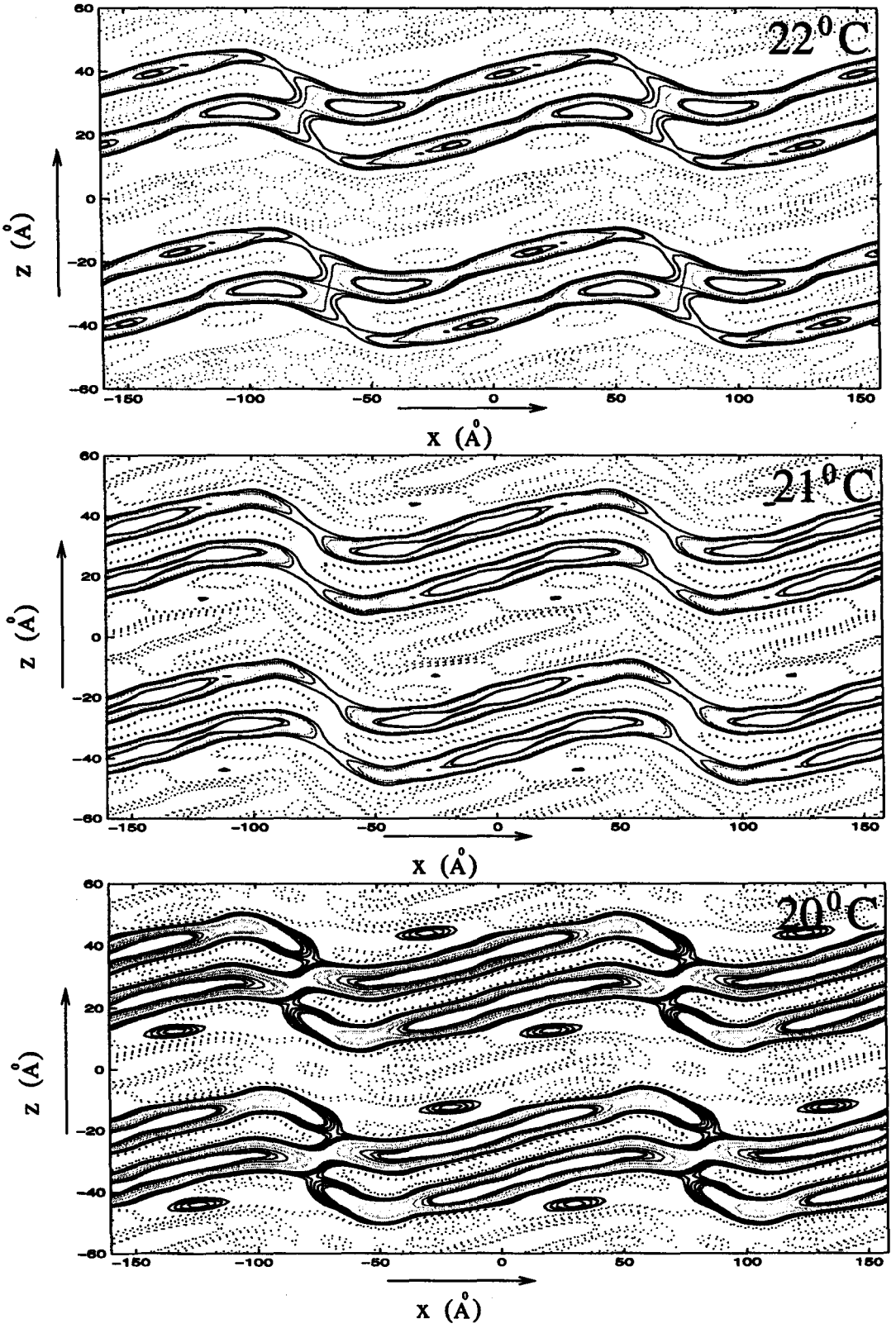

Figure 3.5: **Continuation of figure 3.4.**

3.4 Electron density maps of POPC, DHPC and DLPC

3.4.1 POPC: structural features and temperature dependence

The head-group and the linkage group in POPC is the same as that in DMPC but the chains have 18 and 16 carbon each and the 18 carbons long chain has a double bond. Thus POPC differs considerably from DMPC in the chain region. The electron density map of the ripple phase of POPC at different temperatures and 75% RH is shown in figure-3.6. This data-set is from oriented samples. The converged values of the fitted model parameters are given in table-3.6 and the observed and calculated structure factors corresponding to the figure are given in table-3.7. For these fits, the values of Σ and R are about 1000 and 0.3 respectively. The ripple shape is very similar to that of DMPC. Like DMPC, POPC ripples also have a saw-tooth shape and an offset between the monolayers indicating an average tilt in the direction of rippling. In POPC, the angle γ is much larger than in DMPC, whereas the wavelength and layer spacing are comparable. Unlike those of DMPC, the structural features of the ripple phase of POPC vary significantly with temperature, as shown in table-3.8. The fits are not as good as in the case of DMPC data of ref. [15]. Hence the values of the last two parameters quoted in the table are the ones estimated from the electron density maps. The layer spacing decreases slowly and γ increases steadily as temperature is increased. The ripple wavelength first decreases and then suddenly increases to a large value just below the transition. These trends are very similar to those seen in DPPC [18], but in POPC the temperature dependence is very much pronounced. The amplitude, except near the L_α transition, is about 10 Å, half that in DMPC.

The double bond in one of the chains of POPC is known to lead to a kink in the chain when it goes to the fully stretched conformation. This results in lower main transition temperatures of such lipids. It is interesting that this feature does not seem to affect the structure of the $P_{\beta'}$ phase. It is likely that as proposed by Cevc

Table 3.6: **Converged values of the fitted parameters for the ripple phase of POPC at 75%RH.**

T (°C)	λ_1(Å)	A_r(Å)	ψ	ρ_H/ρ_M	L(Å)
13.0	169.0	15.9	0.0°	1.3	38.8
13.5	127.3	13.9	0.5°	1.5	50.4
14.0	121.7	12.0	0.6°	1.4	51.2

Table 3.7: **The observed and calculated structure factors for POPC oriented sample at different temperatures.**

		13°C		13.5°C		14°C		14.5°C		15°C	
h	k	$\|F_o\|$	F_c	$\|F_o\|$	F_c	$\|F_o\|$	F_c	$\|F_o\|$	F_c	$\|F_o\|$	F_c
1	0	100.0	-56.7	100.0	-100.6	100.0	-89.3	100.0	-95.8	100.0	-53.9
1	-1	28.5	-12.5	42.9	-27.9	29.8	-20.8	23.4	-6.9	7.9	0.7
1	1	26.4	21.3	39.8	29.8	27.6	22.2	20.7	22.7	8.5	-0.5
2	0	18.1	-38.1	22.0	-25.8	23.0	-30.8	22.7	-28.6	16.4	-92.0
2	-1	7.7	-52.8	11.6	-19.1	6.7	-7.3	-	-	3.2	3.5
3	0	11.6	8.9	14.9	14.2	19.1	17.9	21.0	18.2	15.9	19.1
3	-1	19.6	31.5	29.4	28.3	22.6	21.9	18.2	29.1	3.9	-0.3
3	1	7.0	-7.2	10.6	-13.7	14.2	-14.0	14.3	6.5	4.6	-0.8
3	2	10.8	5.2	16.3	13.7	16.4	13.0	9.4	-15.7	-	-
4	0	10.3	5.2	13.6	-6.2	36.1	-24.9	58.5	-58.8	35.1	5.3
4	-1	70.5	-32.9	106.1	-107.2	87.0	-95.9	77.9	-79.0	11.5	2.3
4	-2	28.1	-5.3	42.2	-41.9	26.8	-19.0	14.1	7.7	23.5	-0.8
4	1	19.8	1.1	29.8	24.2	28.2	29.9	26.8	26.3	10.6	-0.4
4	2	16.4	-6.1	24.6	-33.7	14.5	-31.9	9.0	-11.7	4.5	0.0
5	0	7.0	14.4	9.3	-5.3	9.5	-0.5	7.5	7.9	4.8	-0.3
5	-1	9.4	-50.3	14.1	22.7	11.8	16.2	13.7	-14.4	-	-
6	0	7.0	-7.5	-	-	-	-	7.0	6.6	4.8	5.9
6	-1	9.3	10.0	-	-	13.6	-11.8	17.0	12.2	-	-
6	-2	16.8	20.5	-	-	13.1	-14.8	12.6	3.9	-	-

[22], the terminal region of the chain after the double bond is always in a molten conformation.

3.4.2 Oriented sample of DHPC

The main difference between DMPC and DHPC is that in DHPC the chains are connected to the backbone through ether rather than ester linkages. The crystallographic parameters at 37° C and 95±2% RH are: λ_r= 140.9 Å, d=62.3 Å and γ=100°. The temperature dependence of these parameters is negligible. The electron density map is given in figure-3.7. Though the map is not as good as the one obtained for DMPC,

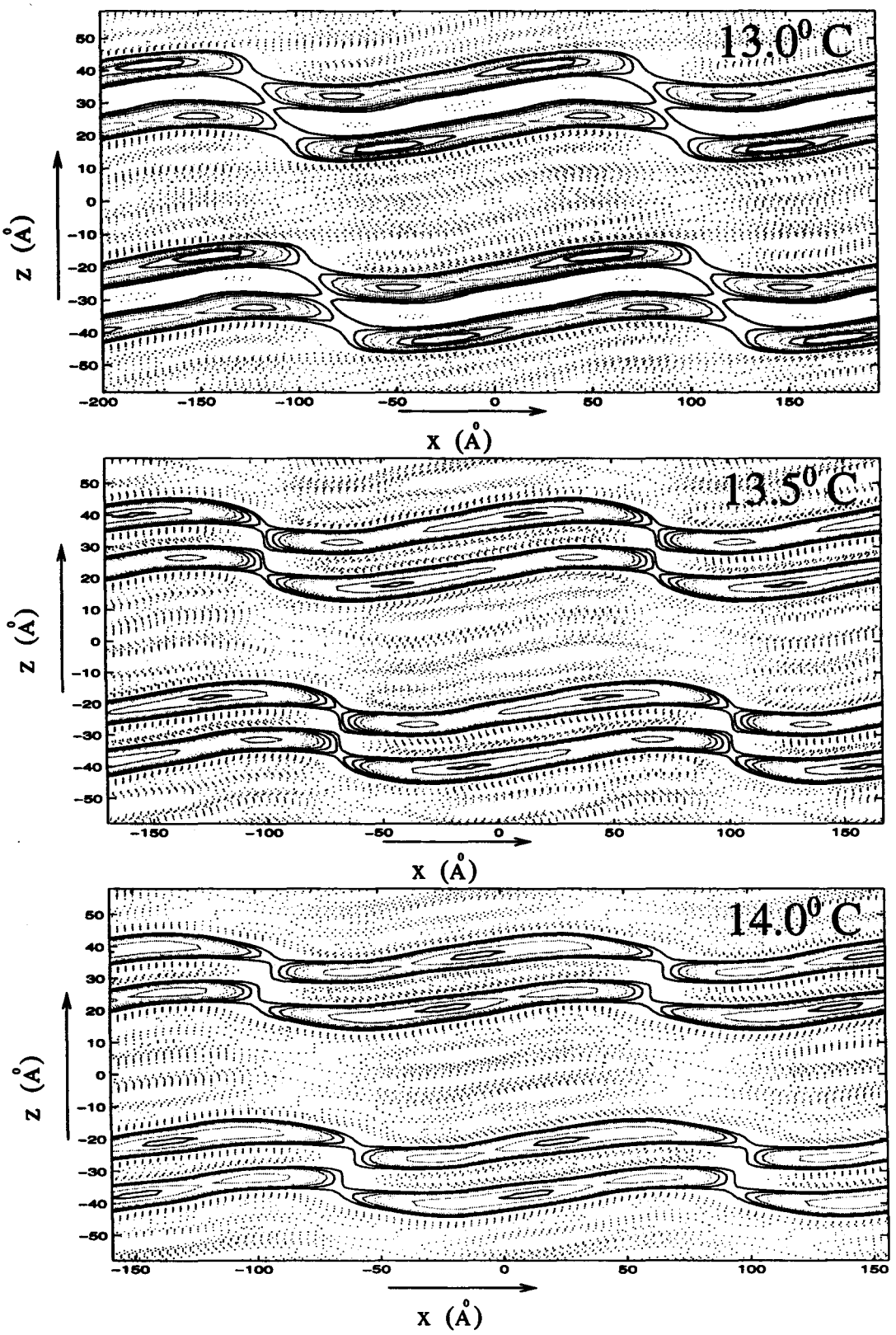

Figure 3.6: **Electron density map of POPC at different temperatures.** The positive (negative) contours are represented by solid (dotted) lines. The regions with positive electron density correspond to the head-groups. Note that the thickness of the bilayers is about 40 Å, whereas that of the water region is about 15 Å.

Table 3.8: **Temperature variation of the structural parameters of the ripple phase of POPC at 75%RH.** From the electron density maps.

T(°C)	d(Å)	γ^o	λ_r (Å)	A_r (Å)	$\frac{\lambda_1}{(\lambda_r-\lambda_1)}$
13.0	58.3±0.1	116±1	200±2	10±1	2.0±0.1
13.5	58.0	119	170	9	1.8
14.0	58.0	120	159	9.0	1.9
14.5	57.3	124	143	5	2.6
15.0	56.4	133	266	5	1.9

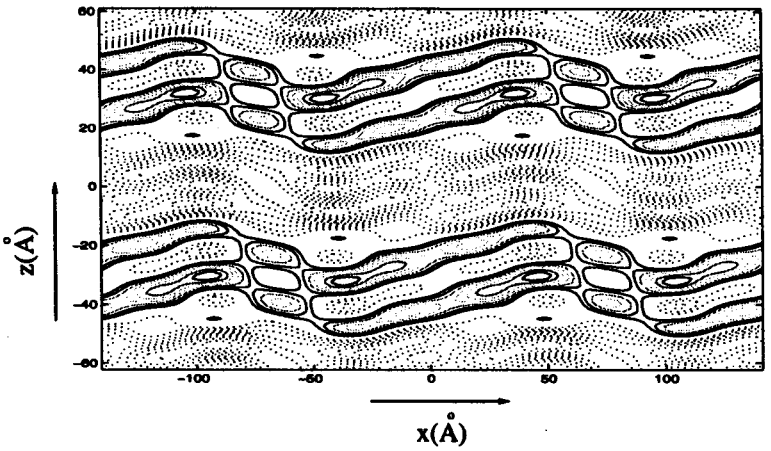

Figure 3.7: **Electron density map of DHPC at 37°C and ≈ 97% RH.** The positive (negative) contours are represented by solid (dotted) lines. The regions with positive electron density correspond to the head-groups. Note that the thickness of the bilayers is about 40Å, whereas that of the water region is about 15 Å.

it can be seen that the general shape is again a saw-tooth with the two arms unequal. The map is consistent with a tilt of the chains along the rippling direction. The observed and calculated structure factors are given in table-3.9 and the converged values of the fitted parameters are given in table 3.10. The value of Σ for this fit is about 5000 and the R-factor is 0.6. In all the compounds discussed so far that is, DMPC, POPC and DHPC, the ratio of the projected lengths of the major and minor arms is about 2 and is essentially insensitive to temperature. This observation further supports the view that the chain organization in the minor arm is not like that in the L_α phase.

Table 3.9: **The observed and calculated structure factors for oriented sample at of DHPC at 37° C and 95±2% RH.**

h	k	$\|F_o\|$	F_c	h	k	$\|F_o\|$	F_c
1	0	100.0	-50.8	3	-3	2.6	-0.6
1	-1	18.1	-24.8	3	3	2.6	-8.4
1	1	12.4	19.5	3	-4	4.2	-0.3
1	-2	6.6	1.5	3	4	4.2	6.9
1	2	6.6	-10.2	4	0	26.3	15.6
1	-3	5.7	1.7	4	-1	8.1	-31.0
1	3	5.7	4.5	4	1	4.7	-0.8
2	0	10.8	-14.7	4	-2	44.2	-52.2
2	-1	16.2	-20.1	4	2	4.7	-12.6
2	1	9.1	15.4	4	-3	5.7	-10.8
2	-2	4.7	-3.8	4	3	22.1	21.2
2	2	4.7	-14.4	4	-4	4.2	8.4
2	-3	5.7	1.8	4	4	4.2	-23.0
2	3	3.6	11.1	5	0	1.3	0.9
3	0	14.1	0.3	5	-1	2.1	-0.1
3	-1	13.5	11.4	5	1	2.1	-1.4
3	1	3.3	-5.0	6	0	1.4	0.0
3	-2	17.9	6.4	7	0	1.5	-8.7
3	2	3.6	7.8				

Table 3.10: **The converged values of the fitted parameter for DHPC**

λ_1(Å)	A_r(Å)	ψ	ρ_H/ρ_M	L(Å)
96.2 Å	20.5 Å	9.6°	1.0	46.2 Å

Table 3.11: **The temperature dependence of the ripple parameters in 1:1 (wt%) mixture of DHPC and DPPC**

T(°C)	d(Å)	γ^o	λ_r(Å)
26	60 ± 2	94 ± 2	175 ± 5
30	60	94	157
34	62	98	147
38	62	99	151
42	58	95	132

Mixture of DHPC and DPPC

The phase diagram of mixtures of DHPC and DPPC has been studied by Lohner et. al. [23]. These mixtures exhibit the $P_{\beta'}$ phase over a larger temperature range than the pure systems; the range being maximum ($\approx 20^o$) for the 1:1 mixture. Since this seems to be largest temperature range of the $P_{\beta'}$ phase, we have studied the temperature dependence of the ripple parameters in the 1:1 (wt.%) mixture. There were too few reflections, probably due to inherent disorder in the system, to do the kind of analysis that we have done for the pure samples. However, the crystallographic parameters can still be computed and are given in table-3.11. The values of the ripple parameters for the mixture are close to the values observed for the pure systems. The layer spacing (d) and the angle γ are insensitive to variations in temperature, whereas the wavelength decreases from a large value near the pre-transition to a value comparable to that in DPPC at higher temperatures.

3.4.3 Unoriented sample of DLPC

DLPC is similar to DMPC except that the chains are shorter (12 carbons). We have phased the data of Tardieu et. al. [1] from unoriented sample of DLPC at -7°C and containing 77% by weight of water. The ripple parameters are: λ_r=85.3Å, d= 51.9Å and γ=110°. Figure-1.10 (chapter-I) shows the electron density map calculated using the phases originally assigned by Tardieu et. al. and figure-3.8 shows the map calculated using our modeling and fitting approach (the corresponding phases are given in table-3.12). The model parameters are given in table-3.13. For this fit, the

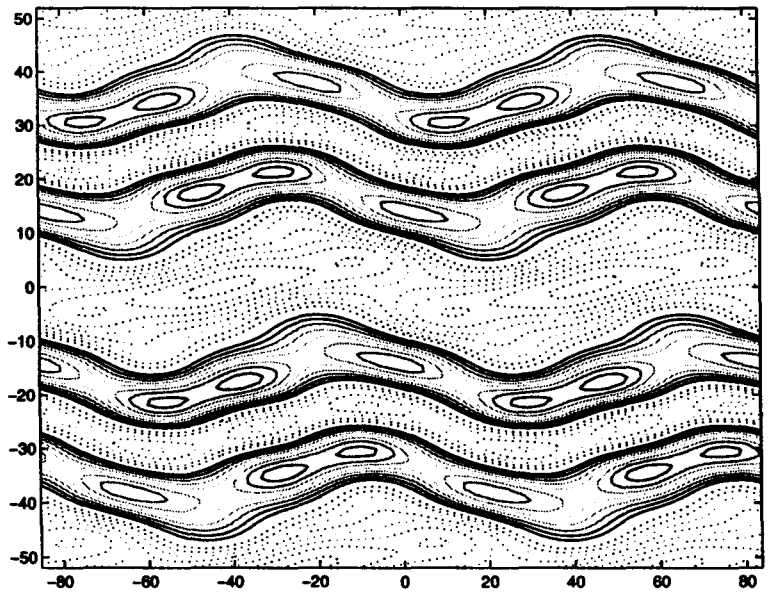

Figure 3.8: **Electron density map of DLPC at -7°C and 77% by weight of water, using the phases calculated by the modeling and fitting procedure.**Data from ref.- [1]

value of Σ is about 100 and the R-factor is about 0.2. The new set of phases leads to a more uniform thickness of the head-group region and is thus probably closer to the correct set. The bilayers in this case have a triangular shape. The major and the minor arms are more or less of equal length. But the ripple profile still lacks a mirror plane normal to the rippling direction because the thickness of the two arms are not equal. The electron density in the head-group region is again higher in the thicker arm and the value of the model parameter L is comparable to twice the length of a fully stretched DLPC molecule (32.6 Å). Thus the structure of this system is also consistent with the presence of an average chain tilt along the rippling direction.

3.5 Influence of chirality

To check the influence of chirality on the ripple phase, the electron density maps of *l* and *dl*-DMPC under similar experimental conditions have been calculated. The observed and calculated structure factors for *l* and *dl*-DMPC at different temperatures and 98±2% RH are given in table-3.14. Almost all the phases of the corresponding reflections in the two cases are the same. The electron density profiles at 24°C for

Table 3.12: **The observed structure factors (F_o), the corresponding phases reported in ref. [1] (Φ_{rep}) and the phases calculated by us (Φ_{cal}).**

h	k	F_o	Φ_{rep}	Φ_{cal}	h	k	F_o	Φ_{rep}	Φ_{cal}
0	1	5.5	-1	-1	2	1	19.1	-1	+1
1	0	36.4	-1	-1	2	2	6.9	+1	-1
1	-1	10	+1	-1	3	-1	16.3	-1	+1
0	2	3.2	+1	+1	3	-2	10	+1	+1
1	1	5.5	-1	+1	3	0	5.7	+1	+1
1	-2	3.9	-1	-1	3	1	9.7	+1	-1
2	-1	22.4	+1	-1	3	2	8.3	+1	+1
1	2	3.0	+1	-1	4	-1	9.6	+1	-1
2	0	30	-1	-1	4	0	7.6	-1	-1
2	-2	21	-1	-1					

Table 3.13: **The converged values of the fitted parameter for DLPC**

λ_1(Å)	A_r(Å)	ψ	ρ_H/ρ_M	L(Å)
39.4 Å	11.5 Å	18.2 ^{o}	1.2	34.6 Å

l and dl-DMPC are presented in figures 3.9 and 3.10. The structural parameters of the ripple phase at two different temperatures are given in table-3.15. As one can observe, the ripples formed by chiral and racemic DMPC bilayers do not differ appreciably. The peak-to-peak amplitude in both cases is approximately 18 Å, and the ratio of the length of the major arm to that of the minor arm is found to be 2.1 and 2.4 for *l*-DMPC and *dl*-DMPC bilayers, respectively. Furthermore, the thickness of the bilayer in the two arms is different in both cases. This can be explained, as discussed before, in terms of an average tilt of the hydrocarbon chains along the ripple wave-vector. Thus at all temperatures studied, the structure of the ripple phase in chiral and racemic DMPC bilayers is practically identical.

3.6 Conclusion

We have calculated the electron density maps of the ripple phase of DMPC, POPC, DHPC and DLPC. The shape of the ripples in these systems are very similar and all of them exhibit asymmetric ripples that lack a plane of reflection normal to the ripple wave-vector. We do not see any temperature dependence of the shape of the

Table 3.14: **The observed and calculated structure factors at 24°C and 98% RH of chiral and racemic DMPC.**

		l-DMPC		dl-DMPC	
h	k	$\|F_o\|$	F_c	$\|F_o\|$	F_c
1	0	100.0	-80.2	100.0	-117.1
1	-1	42.5	-38.0	59.2	-32.9
2	0	29.7	-19.8	65.0	-43.3
2	-1	43.6	-40.5	68.0	-55.2
2	-2	9.3	-15.4	29.0	-38.5
2	2	15.7	-14.6	21.7	-3.2
2	3	10.6	7.9	10.6	0.3
3	0	21.2	-2.9	32.9	11.5
3	-1	42.4	33.9	53.3	39.3
3	-2	29.2	32.0	35.0	38.3
3	2	9.5	17.1	9.0	16.0
3	3	16.5	-15.9	12.3	-0.5
3	4	16.3	10.3	13.3	2.0
3	5	12.4	-4.2	-	-
4	0	29.9	27.9	31.1	22.5
4	-1	25.5	-31.2	33.1	-37.4
4	-2	55.5	-79.5	56.8	-57.5
4	-3	27.7	-33.9	27.9	-35.8
5	0	8.5	0.6	9.6	4.6
5	-1	5.9	0.8	12.0	-0.3
5	-2	7.8	-10.1	10.8	-29.4
6	0	4.4	1.2	6.4	-5.6
6	-1	5.9	-5.4	-	-
7	0	-	-	5.5	-2.2
9	0	-	-	4.5	-1.3

Table 3.15: **The structural parameters of the ripple phase of chiral and racemic DMPC.**

		$\gamma(^o)$	λ(Å)	d	λ_1(Å)	A_r(Å)
l-DMPC	24 ° C	99±1	142±2	56±1	97±2	18±1
	21 ° C	99	145	56	98	18
dl-DMPC	24 ° C	98	141	56	100	19
	21 ° C	98	140	56	99	18

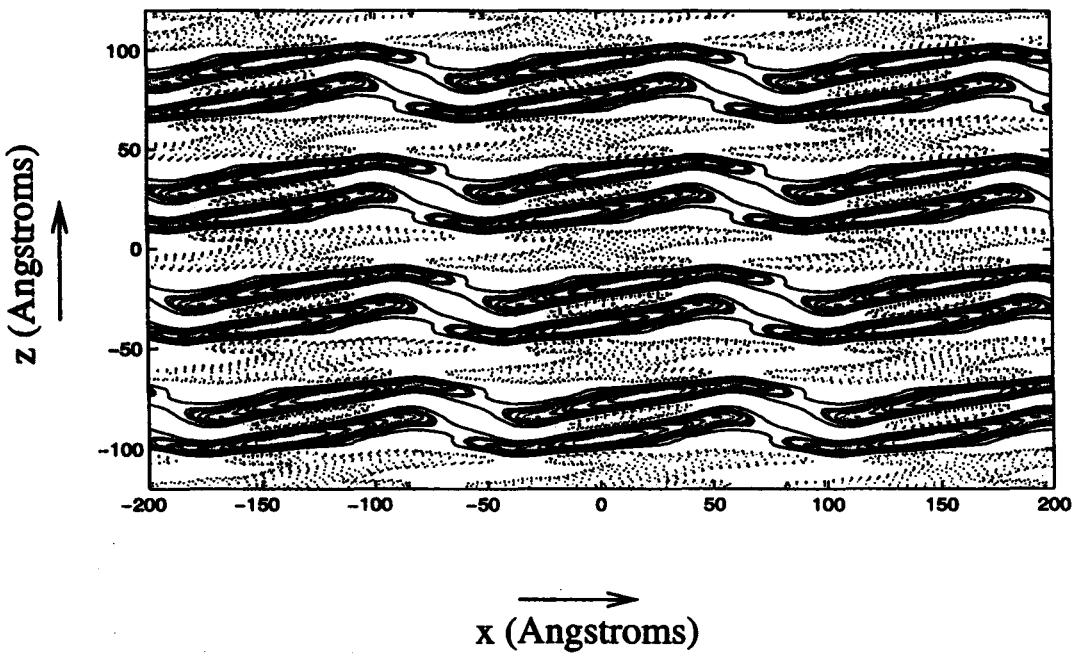

Figure 3.9: **Electron Density Map of the ripple phase of dl-DMPC at 24°C and 98% RH.**The positive (negative) contours are represented by solid (dotted) lines. The regions with positive electron density correspond to the head-groups. Note that the thickness of the bilayers is about 40 Å, whereas that of the water region is about 15 Å.

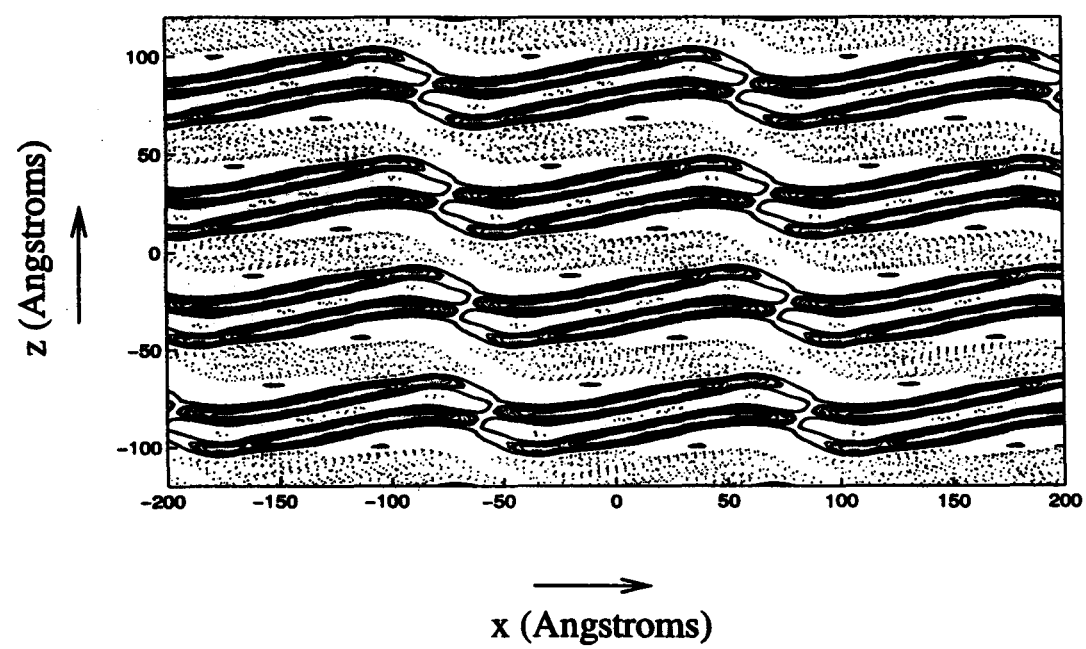

Figure 3.10: **Electron Density Map of ripple phase of l-DMPC at 24°C and 98% RH.**

ripples though the values of the structural parameters do vary with temperature. The structural parameters of DMPC has a very weak temperature dependence whereas in case of POPC the dependence is rather strong.

From our analysis, we have been able to establish the existence of an average chain tilt in the direction of rippling, which is probably responsible for the asymmetric ripples seen in these systems. Such a structure is supported by the electron density maps of all the systems studied. The height profile of the bilayers in DMPC, POPC and DHPC has a saw-tooth shape. The width of the shorter arm is comparable to the bilayer thickness. In DLPC the height profile is closer to triangular, with the width of the two arms almost equal and comparable to the bilayer thickness. It is interesting that the wavelength of the ripples in DLPC ($\approx$ 80 Å) is the lowest reported in the literature. From our result it looks as if the minimum width of an arm of the ripple is set by the bilayer thickness. In that case, a value of about 80 Å may be the lowest possible for the wavelength of the ripples.

We have presented electron density profiles of chiral and racemic DMPC bilayers in the ripple phase. All the structural features in the two cases are found to be practically identical under similar experimental conditions. In particular, the ripples are asymmetric in both these systems. The present study thus unambiguously confirms that the structure of the $P_{\beta'}$ phase does not depend on the chirality of the lipid molecules constituting the bilayer.

Bibliography

[1] A. Tardieu, V. Luzzati, and F. C. Reman, J. Mol. Biol. **75**, 711 (1973).

[2] M. J. Janiak, D. M. Small, and G. G. Shipley, J. Biol. Chem. **254**, 6068 (1979).

[3] P. Pinta da Silva, J. Microsc. **12**, 185 (1971);
A. J. Verkleij, P. H. J. Ververgaert, L. L. M. Van Deenen and P. F. Elbers, Biochim. Biophys. Acta **288** 326 (1972);
P. H. J. Ververgaert, A. J. Verkleij, P. F. Elbers and L. L. M. Van Deenen , Biochim. Biophys. Acta **311** 320 (1973).

[4] H. Yao, S. Matuoka, B. Tenchov, and I. Hatta, Biophys. J. **59**, 252 (1991).

[5] D. Ruppel and E. Sackmann, J. Phys. (Paris) **44**, 1025 (1983).

[6] M.P. Hentschel and F. Rustichelli, Phys. Rev. Lett. **66** 903 (1991).

[7] R.J. Wittebort, C.F. Schmidt, and R.G. Griffin, Biochemistry **20**, 4223 (1981).

[8] M.B. Schneider, W.K. Chan, and W.W. Webb, Biophys. J. **43**, 157 (1983).

[9] K. Lohner, A. Schuster, G. Degovics, K. Muller and P. Laggner, Chem. Phys. Lipids **44** 61 (1987).

[10] S. Kirchner and G. Cevc, Europhys. Lett. **28** 31 (1994).

[11] T. C. Lubensky and F. C. MacKintosh, Phys. Rev. Lett. **71**, 1565 (1993).

[12] C.-M. Chen, T.C. Lubensky, and F.C. MacKintosh, Phys. Rev. E **51**, 504 (1995).

[13] U. Seifert, J. Shillcock and P. Nelson, Phys. Rev. Lett. **77**, 5237 (1996).

[14] W.-J. Sun, S. Tristram-Nagle, R. M. Suter, and J. F. Nagle, Proc. Natl. Acad. Sci. USA **93,** 7008 (1996).

[15] D. C. Wack and W. W. Webb, Phys. Rev. A **40,** 2712 (1989).

[16] J. M. Carlson and J. P. Sethna, Phys. Rev. E **36**, 3359 (1987).

[17] J. T. Woodward and J. A. Zasadzinski, Phys. Rev. E **53**, R3044 (1996).

[18] Y. Inoko, T. Mitsui, K. Ohki, T. Sekiya, and Y. Nozawa, Phys. Stat. Sol. (a) **61**, 115 (1980).

[19] J. Katsaras and V. A. Raghunathan, Phys. Rev. Lett. **74**, 2022 (1995).

[20] J. Katsaras, R. F. Epand, and R. M. Epand, Phys. Rev. E **55**, 3751 (1997).

[21] W. -J. Sun, R. M. Suter, M. A. Knewtson, C. R, Worthington, S. Tristam-Nagle, R. Zhang and J. F. Nagle, Phys. Rev. E **49**, 4665 (1994).

[22] G. Cevc, Biochemistry **30**, 7186 (1991).

[23] K. Lohner, A. Schuster, G. Degovics, K. Muller and P. Laggner, Chem. Phys. Lipids **44** 61 (1987).